

Received 11 May 2020; revised 20 July 2020; accepted 22 July 2020. Date of publication 4 August 2020; date of current version 14 August 2020.  
The review of this article was arranged by Editor C. C. McAndrew.

Digital Object Identifier 10.1109/JEDS.2020.3014133

# Vertical GaN-on-GaN Schottky Barrier Diodes With Multi-Floating Metal Rings

TSUNG-HAN YANG<sup>ID</sup>, HOUQIANG FU<sup>ID</sup> (Member, IEEE), KAI FU<sup>ID</sup>, CHEN YANG<sup>ID</sup>, JOSSUE MONTES,  
XUANQI HUANG<sup>ID</sup>, HONG CHEN, JINGAN ZHOU<sup>ID</sup>, XIN QI<sup>ID</sup>, XUGUANG DENG,  
AND YUJI ZHAO (Member, IEEE)

School of Electrical, Computer, and Energy Engineering, Arizona State University, Tempe, AZ 85287, USA

CORRESPONDING AUTHOR: T.-H. YANG (e-mail: tyang66@asu.edu)

This work was supported by ARPA-E PNDIODES Program monitored by Dr. Isik Kizilyalli.

**ABSTRACT** Vertical GaN Schottky barrier diodes (SBDs) with floating metal rings (FMRs) as edge termination structures have been fabricated on bulk GaN substrates. Devices with different FMR geometries were investigated including various numbers of rings and various spacings between rings. These devices have a low  $R_{on}$  of  $1.16 \sim 1.59 \text{ m}\Omega\cdot\text{cm}^2$ , a turn-on voltage of  $0.96 \sim 0.94 \text{ V}$ , a high on-off ratio of  $10^9$ , a nearly ideal ideality factor of  $1.03 \sim 1.09$ , and a Schottky barrier height of  $1.11 \sim 1.18 \text{ eV}$  at room temperature. These devices have similar forward electrical characteristics, indicating that FMRs don't degrade the device rectifying performance. The ideality factor decreased and the Schottky barrier height increased with increasing temperature from 300 K to 420 K, where the temperature dependencies of the two parameters indicate the inhomogeneity of the metal/semiconductor Schottky interface. In addition, FMRs can improve device breakdown voltages. As the number of FMRs increased from 0 to 20, the reverse breakdown voltage increased from 223 to 289 V. As the spacing between the FMRs increased from 1.5 to 3  $\mu\text{m}$ , the reverse breakdown voltage increased from 233 to 290 V, respectively. These results indicate multiple FMRs with proper spacings can effectively improve breakdown performance without degrading the device forward characteristics. This work represents a useful reference for the FMR termination design for GaN power devices.

**INDEX TERMS** Gallium nitride, power electronics, wide band-gap semiconductor, Schottky barrier diode, edge termination, floating metal ring.

## I. INTRODUCTION

Gallium nitride has been widely used in both electronic and photonic devices [1]–[7]. It is an ideal candidate for high power and high-frequency applications due to its wide bandgap ( $\sim 3.4 \text{ eV}$ ), high critical electric field ( $> 3 \text{ MV/cm}$ ), and high Baliga's figure of merit (BFOM). Conventional lateral GaN power devices have been grown and fabricated on foreign substrates such as sapphire [8], [9] and silicon [4], [10]–[12], which showed limited performance. This is because lateral geometry results in surface-related issues, poor thermal dissipation, and limitations on current and voltage ratings. The second reason is related to the heteroepitaxial growth which gives rise to high defect densities and thermal coefficient mismatch. Recently, bulk GaN substrates have been commercialized that can enable vertical GaN

power devices with much lower defect densities, less stringent requirements on thermal managements, better immunity to surface states and higher currents and voltages [13]–[19]. GaN Schottky barrier diodes have been widely investigated due to low turn-on voltages, fast switching, and lack of reverse recovery charges.

One of the key topics of GaN power diodes is to eliminate or alleviate the electric field crowding effects at the junction edge to avoid device premature breakdown, thus achieving high breakdown voltages. Several edge termination methods have been reported, such as field plates, trench structures, and deep mesa etching [20]–[24]. Floating metal rings (FMRs) are another effective and easy-to-implement termination method [15], [25]. It has been shown that FMRs can effectively reduce electric field concentrations of the

main Schottky junction due to the expansion of the depletion layer along the FMRs [26]. This method has also been adopted in SiC [26], [27] and Ga<sub>2</sub>O<sub>3</sub> [28] Schottky barrier diodes. Another advantage of this method is that FMRs are very easy to implement. Unlike other edge termination techniques which require complicated fabrication processes, FMRs can be formed simultaneously with the Schottky contact without additional fabrication steps, simplifying device fabrication and reducing costs. In this work, we demonstrate the FMR termination structure on vertical GaN-on-GaN Schottky barrier diodes with different FMR geometry designs. The devices have similar forward characteristics and nearly ideal ideality factors. With optimized FMR structures, device breakdown performance was improved. These results can serve as helpful references for the future development of power GaN devices.

## II. DEVICE FABRICATION

The samples were grown homoepitaxially by metalorganic chemical vapor deposition (MOCVD) on *c*-plan n<sup>+</sup>-GaN free-standing substrates. Trimethylgallium (TMGa) and ammonia (NH<sub>3</sub>) were used as the gallium (Ga) and nitrogen (N) sources, respectively. N-type dopants Si were incorporated by using silane (SiH<sub>4</sub>) precursors. Figure 1(a) shows the structure schematic of the devices. 1-μm-thick n<sup>+</sup>-GaN with an electron concentration of  $\sim 2 \times 10^{18} \text{ cm}^{-3}$  were first grown on the GaN substrates, followed by 9-μm-thick n-GaN drift layer with an electron concentration of  $\sim 2 \times 10^{16} \text{ cm}^{-3}$ , which was estimated by the capacitance-voltage (C-V) method [29]. High-resolution X-ray diffraction (HRXRD) was used to characterize the crystal quality of the samples. The setup used is the PANalytical X'Pert Pro materials research X-ray diffractometer (MRD) system using Cu K $\alpha$ 1 radiation source with a wavelength of 1.541 Å. The incident beam optics and the diffracted beam optics are the hybrid monochromator and the triple-axis module, respectively. The full width at half maximum (FWHM) of (002) and (102) planes are 44 and 32 arcsec, respectively. The dislocation density can be calculated by using the following equation:

$$D = \frac{\beta_{(002)}^2}{\vec{b}^2} + \frac{\beta_{(102)}^2}{\vec{b}^2} \quad (1)$$

where  $\beta$  is the FWHM and  $\vec{b}$  is the Burgers vector [30]. The first term represents the screw dislocation density, and the second term represents the edge dislocation density. The dislocation density was about  $2.2 \times 10^6 \text{ cm}^{-2}$ , indicating high material quality of the epilayers.

After the material growth, conventional photolithography was then applied to fabricate the devices. Figure 1(b) shows the process fabrication flow. The samples were first cleaned with ultrasonic using acetone and isopropyl alcohol, then rinsed with deionized water. Next, photolithography was used to define the pattern of the contacts. An oxygen plasma treatment was applied to remove residual photoresist, followed

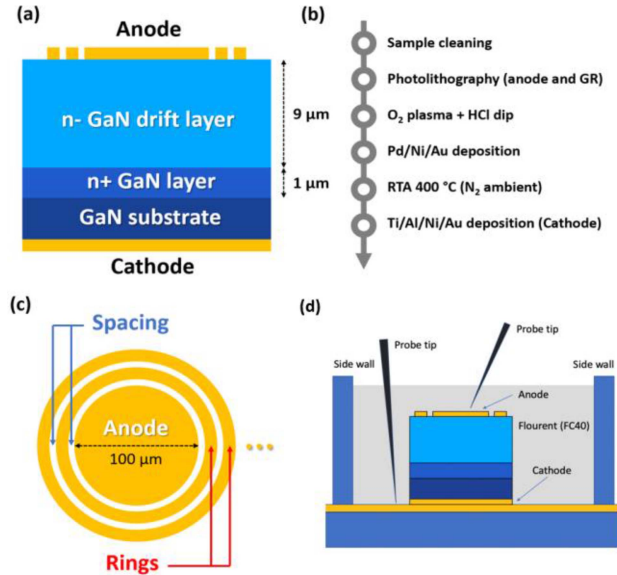


**FIGURE 1.** (a) Structure schematic of the vertical GaN Schottky barrier diodes with multi-floating metal ring termination structure (b) Fabrication process of the device. (c) Top view schematic diagram of the device with rings. (d) Measurement setup with the device immersed in FC40 to avoid breakdown through air.

by 30 seconds soaking in diluted hydrochloric acid (HCl) to remove potential surface oxidization layers. The metal deposition was conducted by electron beam evaporation. Pd/Ni/Au metal stacks were first deposited on the samples to form the anodes and FMRs, followed by rapid thermal annealing (RTA) at 400°C in a nitrogen ambient. Then Ti/Al/Ni/Au metal stacks were then deposited on the backside of the samples to form the cathodes.

Figure 1(c) presents the geometry of the device with FMRs. The anode has a diameter of 100 μm surrounded by multiple FMRs. The number of FMRs varied from 0, 5, 10, to 20, and the spacing between the FMRs varied from 1.5 μm to 3.5 μm with a step of 0.5 μm. The width of the FMRs is 10 μm. Forward current-voltage measurements and reverse breakdown measurements were conducted using Keithley 2400 semiconductor parameter analyzer. Figure 1(d) demonstrates the measurement setup. During the breakdown measurements, the devices were immersed in Fluorinert (FC-40) to avoid flash-over through the air, which may underestimate the actual breakdown voltages.

## III. RESULTS AND DISCUSSION

Figure 2 presents the forward current density-voltage (J-V) curves and the on resistance-voltage (R<sub>on</sub>-V) curves of vertical GaN SBDs with 0, 5, 10, and 20 FMRs in a semi-log scale at room temperature. The spacings were fixed to be 2 μm. The forward voltage was applied at the anode from 0 V to 2 V with a step of 0.02 V with the cathode grounded. The current density was calculated based on the area of the anode. The maximum current densities of these 4 devices at 2 V were about 699, 761, 905, 661 A/cm<sup>2</sup>,

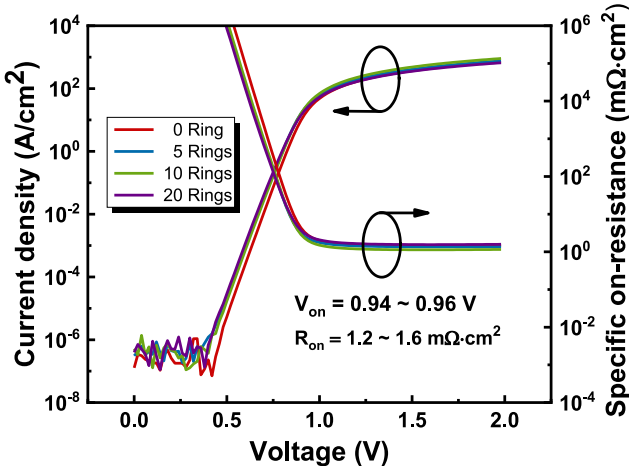


**FIGURE 2.** Forward current density-voltage curve (I-V) of vertical GaN Schottky barrier diodes in a semi-log scale with various floating metal rings at room temperature in a linear scale. The on voltage is around 0.94 ~0.96 V. The specific on resistance is around 1.2~1.6 mΩ·cm<sup>2</sup>. All four devices have a same spacing equal to 2 μm.

**TABLE 1.** Device parameters for the SBDs with various FMRs.

		0 FMR	5 FMRs	10 FMRs	20 FMRs
300 K	Current density @ 2V (A/cm <sup>2</sup> )	699	761	905	661
	Turn-on Voltage (V)	0.96	0.94	0.94	0.94
	Specific on-resistance (mΩ·cm <sup>2</sup> )	1.47	1.37	1.16	1.59
	Ideality factor	1.03	1.09	1.07	1.09
420 K	Schottky barrier height (eV)	1.18	1.12	1.14	1.11
	Ideality factor	1.01	1.03	1.03	1.04
	Schottky barrier height (eV)	1.21	1.20	1.26	1.17

respectively. These devices all had a good on/off ratio of 10<sup>9</sup>. The turn-on voltages of the four devices were extracted by linear exploration, which were about 0.96, 0.94, 0.94, 0.94 V, respectively. The specific on-resistances extracted from the curves were about 1.47, 1.37, 1.16, 1.59 mΩ·cm<sup>2</sup>, respectively. These results indicate that the addition of FMRs doesn't significantly impact the device forward rectifying characteristics.

Figure 3 shows the forward temperature-dependent measurements of these four devices in both linear and semi-log scales. The temperature increased from 300 K to 420 K with a step of 30 K. The relationship between diode currents and voltages can be explained by the thermal emission model, which is described by the following equations [29]:

$$I = I_s \left\{ \exp \left[ \frac{q(V - IR_s)}{nkT} \right] - 1 \right\} \quad (2)$$

$$I_s = AA^*T^2 \exp \left( -\frac{q\phi_b}{kT} \right) \quad (3)$$

where  $I_s$ ,  $V$ ,  $R_s$ ,  $n$ ,  $k$ ,  $T$ ,  $A$ ,  $A^*$ ,  $\phi_b$ , are the saturation current, the applied voltage, the series resistance, the ideality factor, the Boltzmann constant, the device area, the Richardson constant, and the effective Schottky barrier height, respectively. As the temperature increased, the current increased under off-state and decreased under on-state, respectively. This can be explained by the combination effect of the saturation current ( $I_s$ ) and the series resistance ( $R_s$ ). As the temperature increased, the saturation current increased naturally which leads to an increment in the diode current. On the contrary, as the temperature increased, the series resistance increased (due to more scattering) and hence the diode current decreased because of the  $-IR_s$  term in equation (2). When the diode is off, the effect of the series resistance can be neglected since the current level is too small ( $-IR_s \approx 0$ ). When the diode is on, this  $-IR_s$  term needs to be taken into the consideration. Combine both effects, the different trends of the temperature dependence of the current under on/off states can thus be explained. Moreover, the ideality factor and the Schottky barrier height can be calculated as a function of temperature using the following equations:

$$n = \frac{q}{kT} \frac{1}{d(\ln I)/dV} \quad (4)$$

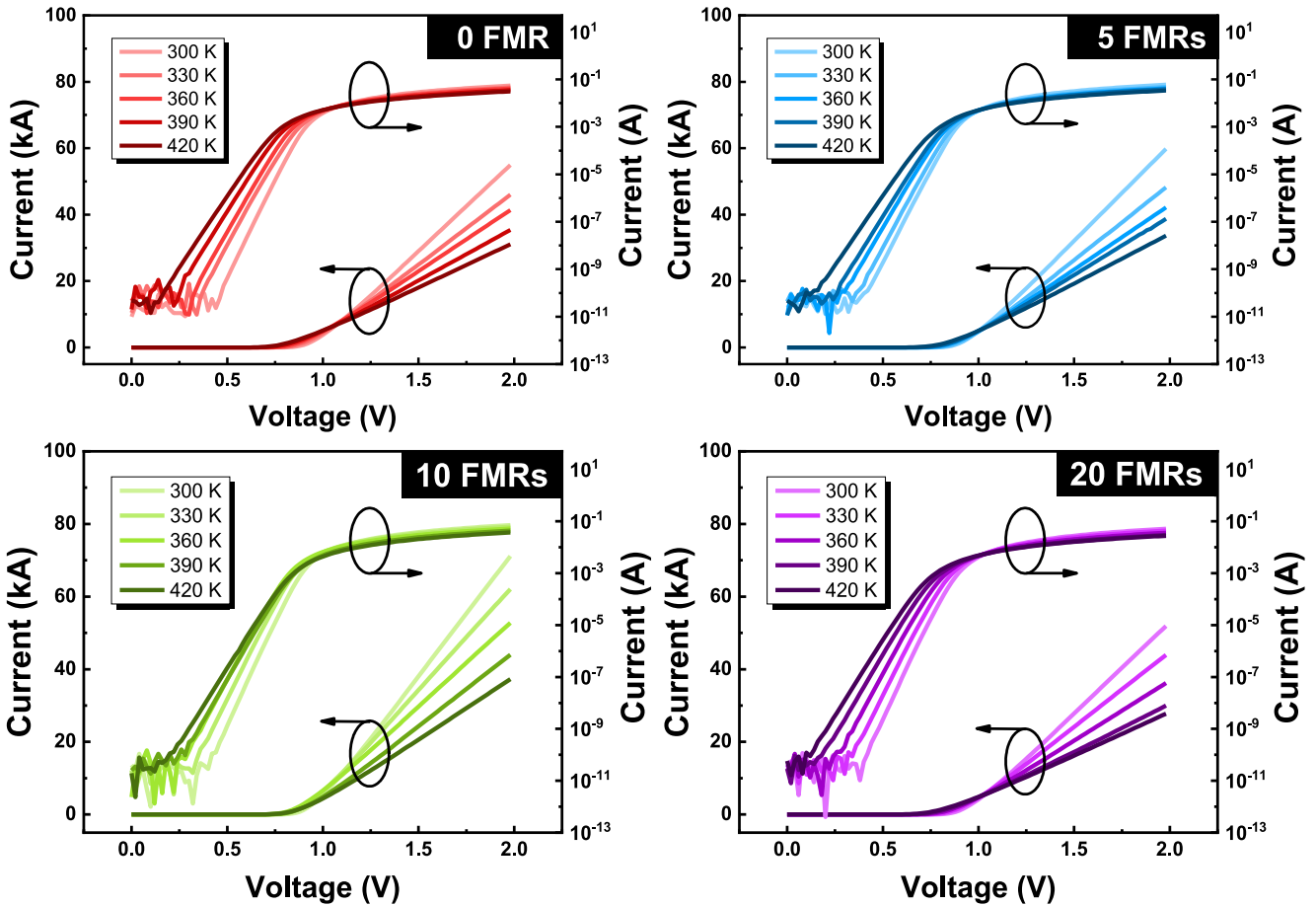
$$\phi_b = -\frac{kT}{q} \ln \left( \frac{I_s}{A^*T^2} \right) \quad (5)$$

Figure 4(a) shows the extracted ideality factors and Schottky barrier heights as a function of temperature for the four devices. As the temperature increased from 300 K to 420 K, the ideality factor slightly decreased from 1.03, 1.09, 1.07, 1.09 to 1.01, 1.03, 1.03, 1.04, respectively, and the Schottky barrier height increased from 1.18, 1.12, 1.14, 1.11 eV to 1.21, 1.20, 1.26, 1.17 eV, respectively. The correlation between the ideality factor and the Schottky barrier height can be further characterized by a well known linear relationship, as shown in Fig. 4(b). The abnormal behavior of the device with 10 rings may stem from measurement errors. This phenomenon has been studied and reported previously in GaN [31]–[33] and other wide bandgap materials, such as Ga<sub>2</sub>O<sub>3</sub> [29] and SiC [34]. The temperature dependence of both the ideality factor and the Schottky barrier height can be explained by the thermionic emission over an inhomogeneous Schottky barrier with a voltage-dependent barrier height. Some non-ideal condition such as rough interface between electrode and semiconductor, metal grain boundaries, and non-uniform metallurgy can lead to this spatial inhomogeneity [35], [36]. To incorporate the barrier inhomogeneity into the thermionic emission model in equation (2), it is assumed that the Schottky barrier has a Gaussian distribution potential with a mean barrier height  $\bar{\phi}_b$  and a standard deviation  $s$ , and the barrier is linearly dependent on voltage:

$$\phi_b = \bar{\phi}_b - \frac{q}{2kT} \sigma^2 \quad (6)$$

$$\bar{\phi}_b = \phi_{b0} + \gamma V \quad (7)$$

$$\sigma^2 = \sigma_0^2 - \xi V \quad (8)$$



**FIGURE 3.** Temperature dependent forward current-voltage (I-V) curves of devices with 0, 5, 10, 20 FMRs in both linear and semi-log scale. The temperature was increased from 300K to 420K with a step of 30 K. The four devices have identical forward electrical performance.

where  $\bar{\phi}_{b0}$  and  $\sigma_0$  are the mean barrier height and the standard deviation when  $V = 0$ . The coefficients  $\gamma$  and  $\xi$  represent the voltage-induced deformation of the Schottky barrier distribution. Note that  $\gamma < 0$  and  $\xi > 0$ , indicating larger voltage can decrease the mean Schottky barrier height and reduce the inhomogeneity of the barrier distribution, respectively [29], [37]. The ideality factor can be expressed as:

$$n^{-1} - 1 = -\gamma - \frac{q}{2kT}\xi \quad (9)$$

This explains why the experimental values of the ideality factor always exceed 1. Figure 4(c) shows the fitting plot of equation (7) and (9) using the average values of these devices. The extracted  $\bar{\phi}_{b0}$  is about 1.41 eV and the extracted  $\sigma_0$  is about 0.12 eV. Previously reported SBDs on different materials showed a similar fluctuation parameter, such as  $\text{Ga}_2\text{O}_3$  (0.14 eV) [29],  $\alpha\text{-IGZO}$  (0.13 eV) [35],  $\text{ZnO}$  (0.134 eV) [38], and  $\alpha\text{-ZTO}$  (0.12 eV) [37]. Moreover, this inhomogeneity modification can be applied into the original thermionic emission model:

$$\ln\left(\frac{I_s}{AT^2}\right) - \frac{q^2\sigma_0^2}{2k^2T^2} = \ln(A^*) - \frac{q\bar{\phi}_{b0}}{kT} \quad (10)$$

Figure 4(d) shows the original and the modified Richardson plot based on the Eqs. (3) and (10), respectively. The extracted original  $A^*$  ( $3.91 \times 10^{-2} \text{ A cm}^{-2} \text{ K}^{-2}$ ) is unreasonably small. However, if we take the inhomogeneity barrier into consideration and use the modified model for the extraction, the value of  $A^*$  ( $33.48 \text{ A cm}^{-2} \text{ K}^{-2}$ ) is close to the theoretical value ( $26 \text{ A cm}^{-2} \text{ K}^{-2}$ ) [39]. Table 1 and figure 5 summarize the forward characteristics of the four devices. These devices have very similar forward performance, even though there are still some trivial differences due to non-uniformity of the material quality and the process fabrication skills, their forward characteristics are still similar enough for a fair comparison of the reverse breakdown performance in the next part.

Figure 6(a) presents the reverse breakdown voltage measurements of these four devices with 2  $\mu\text{m}$  spacings and various numbers of FMRs. The device breakdown was edge breakdown with catastrophic damage at the contact edge as observed by optical microscopy. As the number of the FMRs increased from 0 (reference) to 5, 10, and 20, the average breakdown voltage increased from 223 to 247, 272, and 289 V, which were about 11%, 22%, 30% increment. This increase in breakdown voltages is because FMRs can be

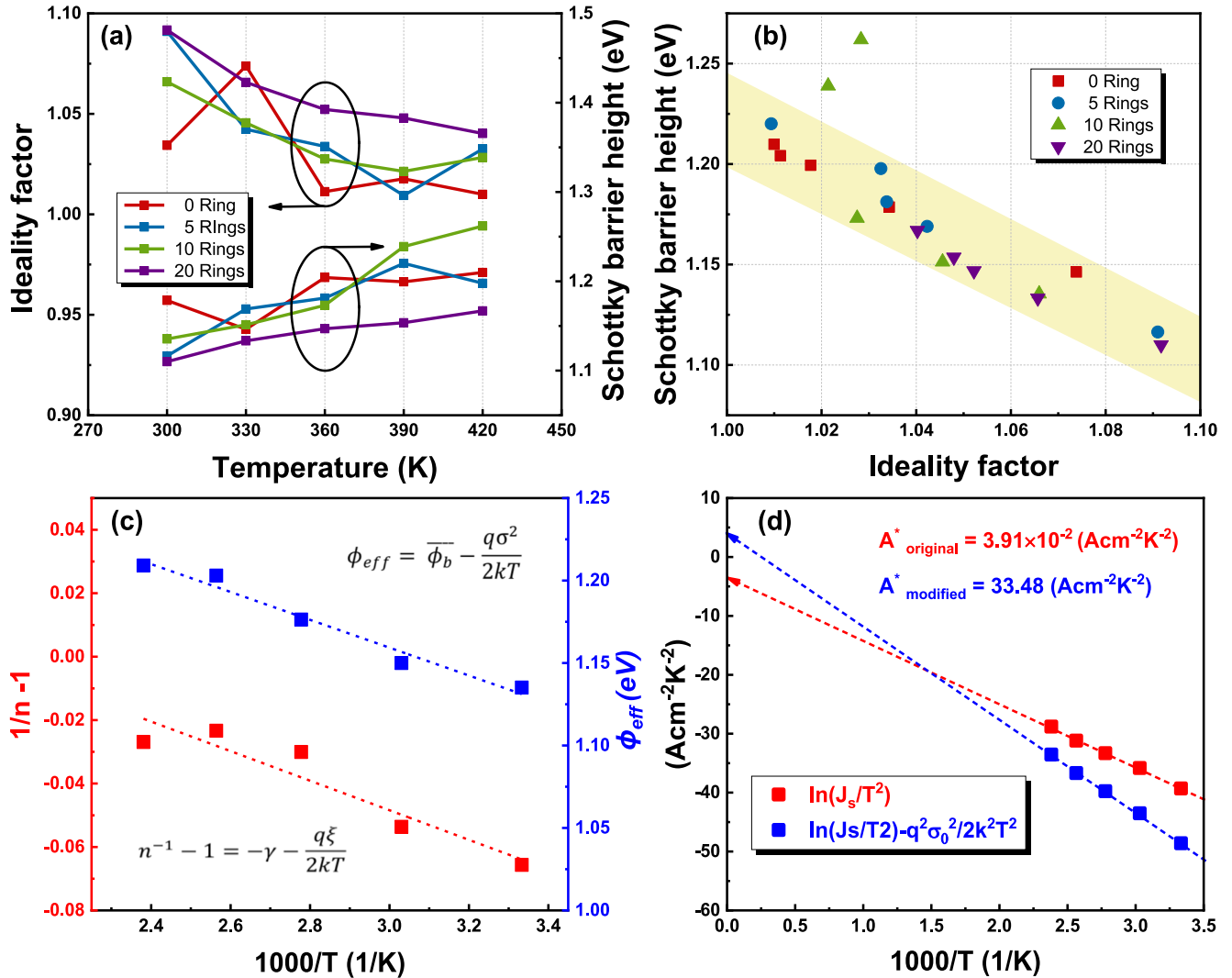


**FIGURE 4.** (a) Ideality factor and Schottky barrier height as a function of temperature from 300 K to 420 K with a step of 30 K. (b) Ideality factor versus Schottky barrier height. (c) Plot of the average effective barrier height and  $n-1-1$  versus  $1000/T$ . (d) Original and modified Richardson plot for GaN SBDs. The dash line shows the fitting curve.

considered as depletion region extension to achieve a smooth potential contour at the device edge. More FMRs can help spread the electric field laterally at the device edge and thus significantly enhance the breakdown voltage.

In addition, the spacing between FMRs is also very critical since it determines the location of the peak electric field. Figure 6(b) shows the reverse breakdown voltage measurements of 5-ring GaN SBDs with various ring spacings from 1.5  $\mu$ m to 3.5  $\mu$ m with a step of 0.5  $\mu$ m. As the spacing increased, the breakdown voltage increased from 233 to 247, 260, 290 and 271 V, about 4%, 11%, 17%, 30%, and 22% increment compared to the reference device (no ring,  $V_{br} = 223$  V). The maximum breakdown voltage of 290 V occurred at the spacing equals to 3  $\mu$ m. At this condition, the depletion region extensions can cover the spacings effectively and hence the electric field can spread widely. This helps lower the peak electric field and thus

reach a higher breakdown voltage. However, when spacing equals to 3.5  $\mu$ m, it is too wide for the depletion region extensions to cover the spacing effectively. As a result, the uniformity and the area of the electric field distribution decreased and hence the breakdown voltage decreased to 271 V. Furthermore, the enhancement effects in breakdown voltages by the FMRs with increasing ring spacing may also decreased afterward. Similar phenomenon happened in reference [15] and [28], too.

In short, although these devices have very similar forward performance, their reverse breakdown performance is very different. More FMRs lead to higher breakdown voltages, indicating that FMRs can effectively alleviate the electrical field crowding around the edge of the anode. In addition, the spacing of the FMRs also plays an important role in the electric field distribution of the devices.



**FIGURE 5.** Device forward characteristics for the SBDs with 0/5/10/20 FMRs. Despite the trivial differences caused by non-uniformity of the material quality and the process fabrication skills, their forward performance is similar enough for a fair comparison of the reverse breakdown measurement.

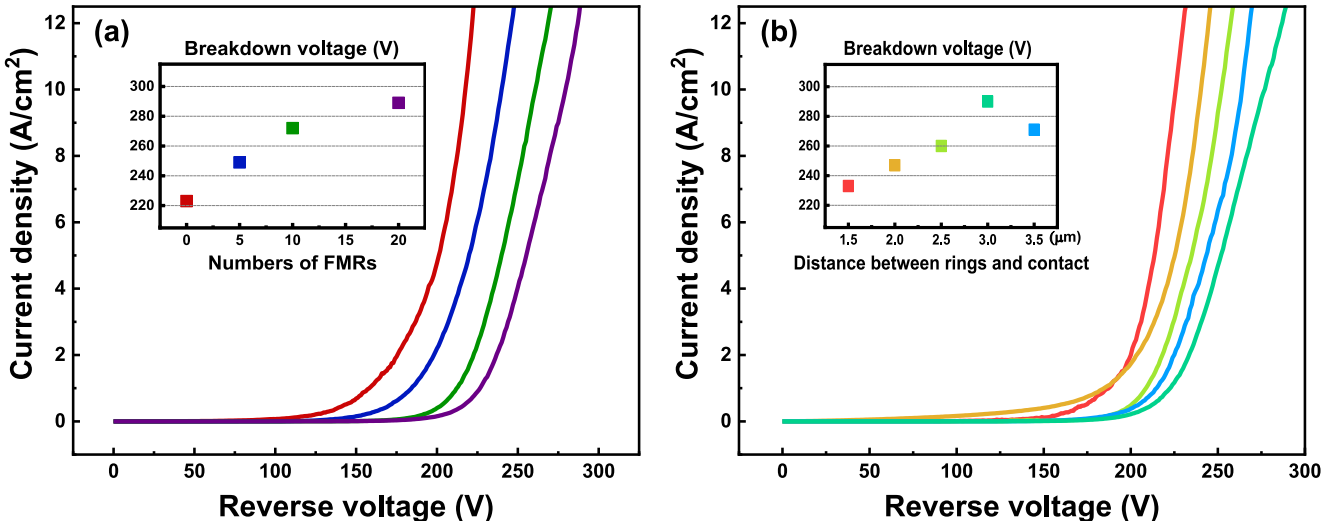


**FIGURE 6.** (a) Reverse breakdown voltage of GaN SBDs with 2  $\mu\text{m}$  spacings and various numbers of floating metal rings (b) Reverse breakdown voltage of GaN SBDs with 5 FMRs and various distance between contact and rings.

#### IV. CONCLUSION

Vertical GaN Schottky barrier diodes with various FMR structures were fabricated on bulk GaN substrates. The devices have a low  $R_{\text{on}}$  of  $1.16 \sim 1.59 \text{ m}\Omega \cdot \text{cm}^2$ , turn-on voltage of  $0.96 \sim 0.94 \text{ V}$ , and a high on-off ratio of  $10^9$ . The ideality factor is about  $1.03 \sim 1.09$ , which is nearly unity and the Schottky barrier height is about  $1.11 \sim 1.18 \text{ eV}$  at room temperature. As the temperature increased to 420 K, the ideality factor decreased and the Schottky barrier height increased. This phenomenon is due to the inhomogeneity of the Schottky barrier. All these devices have very similar forward characteristics, indicating the FMRs don't degrade the device rectifying performance. As the number of the FMRs increased from 0 to 5, 10, and 20, the breakdown voltage increased from 223 to 247, 272, and 289 V, respectively. This indicates more FMRs help distribute the electric field laterally at the device edge and thus enhance the breakdown voltage performance. In addition, as the spacing of the FMRs increased from 1.5  $\mu\text{m}$  to 3.5  $\mu\text{m}$  with a step

of 0.5  $\mu\text{m}$ , the breakdown voltage increased from 233, 247, 260, to 290, then drop to 271 V. The maximum occurred at 3  $\mu\text{m}$  and then decreased afterward. This is because the non-effective depletion region expansion through the wider spacing. These results can serve as important references for the future design of FMR structure on power devices to obtain better breakdown performance.

#### ACKNOWLEDGMENT

The samples are provided by IQE KC, LLC. The authors acknowledge the use of facilities within the Eyring Materials Center at Arizona State University. The devices were fabricated at Nanofab at Arizona State University.

#### REFERENCES

- [1] Y. Zhao, H. Fu, G. T. Wang, and S. Nakamura, "Toward ultimate efficiency: Progress and prospects on planar and 3D nanostructured nonpolar and semipolar InGaN light-emitting diodes," *Adv. Opt. Photon.*, vol. 10, no. 1, pp. 246–308, 2018.

- [2] H. Fu, Z. Lu, X. Huang, H. Chen, and Y. Zhao, "Crystal orientation dependent intersubband transition in semipolar AlGaN/GaN single quantum well for optoelectronic applications," *J. Appl. Phys.*, vol. 119, no. 17, 2016, Art. no. 174502.
- [3] D. Ji *et al.*, "Large-area *in-situ* oxide, GaN interlayer-based vertical trench MOSFET (OG-FET)," *IEEE Electron Device Lett.*, vol. 39, no. 5, pp. 711–714, May 2018.
- [4] Y. Zhang, A. Dadgar, and T. Palacios, "Gallium nitride vertical power devices on foreign substrates: a review and outlook," *J. Phys. D Appl. Phys.*, vol. 51, no. 27, 2018, Art. no. 273001.
- [5] S. Chowdhury and U. K. Mishra, "Lateral and vertical transistors using the AlGaN/GaN heterostructure," *IEEE Trans. Electron Devices*, vol. 60, no. 10, pp. 3060–3066, Oct. 2013.
- [6] I. C. Kizilyalli, A. P. Edwards, O. Aktas, T. Prunty, and D. Bour, "Vertical power pn diodes based on bulk GaN," *IEEE Trans. Electron Devices*, vol. 62, no. 2, pp. 414–422, Feb. 2015.
- [7] H. Fu *et al.*, "High voltage vertical GaN pn diodes with hydrogen-plasma based guard rings," *IEEE Electron Device Lett.*, vol. 41, no. 1, pp. 127–130, Jan. 2020.
- [8] G. T. Dang *et al.*, "High voltage GaN schottky rectifiers," *IEEE Trans. Electron Devices*, vol. 47, no. 4, pp. 692–696, Apr. 2000.
- [9] B. Zhang, T. Egawa, G. Zhao, H. Ishikawa, M. Umeno, and T. Jimbo, "Schottky diodes of Ni/Au on n-GaN grown on sapphire and SiC substrates," *Appl. Phys. Lett.*, vol. 79, no. 16, pp. 2567–2569, 2001.
- [10] Y. Zhang, M. Yuan, N. Chowdhury, K. Cheng, and T. Palacios, "720-V/0.35-mΩ·cm<sup>2</sup> fully vertical GaN-on-Si power diodes by selective removal of Si substrates and buffer layers," *IEEE Electron Device Lett.*, vol. 39, no. 5, pp. 715–718, May 2018.
- [11] S. Mase, T. Hamada, J. J. Freedman, and T. Egawa, "Effect of drift layer on the breakdown voltage of fully-vertical GaN-on-Si pn diodes," *IEEE Electron Device Lett.*, vol. 38, no. 12, pp. 1720–1723, Dec. 2017.
- [12] X. Zou, X. Zhang, X. Lu, C. W. Tang, and K. M. Lau, "Fully vertical GaN pin diodes using GaN-on-Si epilayers," *IEEE Electron Device Lett.*, vol. 37, no. 5, pp. 636–639, May 2016.
- [13] Y. Saitoh *et al.*, "Extremely low on-resistance and high breakdown voltage observed in vertical GaN Schottky barrier diodes with high-mobility drift layers on low-dislocation-density GaN substrates," *Appl. Phys. Exp.*, vol. 3, no. 8, 2010, Art. no. 081001.
- [14] A. M. Ozbek and B. J. Baliga, "Planar nearly ideal edge-termination technique for GaN devices," *IEEE Electron Device Lett.*, vol. 32, no. 3, pp. 300–302, Mar. 2011.
- [15] S.-C. Lee *et al.*, "A new vertical GaN Schottky barrier diode with floating metal ring for high breakdown voltage," in *Proc. IEEE 16th Int. Symp. Power Semicond. Devices ICs*, 2004, pp. 319–322.
- [16] J. Laroche, F. Ren, K. Baik, S. Pearton, B. Shelton, and B. Peres, "Design of edge termination for GaN power Schottky diodes," *J. Electron. Mater.*, vol. 34, no. 4, pp. 370–374, 2005.
- [17] Y. Cao, R. Chu, R. Li, M. Chen, R. Chang, and B. Hughes, "High-voltage vertical GaN Schottky diode enabled by low-carbon metal-organic chemical vapor deposition growth," *Appl. Phys. Lett.*, vol. 108, no. 6, 2016, Art. no. 062103.
- [18] N. Tanaka, K. Hasegawa, K. Yasunishi, N. Murakami, and T. Oka, "50 A vertical GaN Schottky barrier diode on a free-standing GaN substrate with blocking voltage of 790 V," *Appl. Phys. Exp.*, vol. 8, no. 7, 2015, Art. no. 071001.
- [19] Y. Wang *et al.*, "Ultra-low leakage and high breakdown Schottky diodes fabricated on free-standing GaN substrate," *Semicond. Sci. Technol.*, vol. 26, no. 2, 2010, Art. no. 022002.
- [20] K. Ip *et al.*, "High current bulk GaN Schottky rectifiers," *Solid-State Electron.*, vol. 46, no. 12, pp. 2169–2172, 2002.
- [21] M. Zhu *et al.*, "1.9-kV AlGaN/GaN lateral Schottky barrier diodes on silicon," *IEEE Electron Device Lett.*, vol. 36, no. 4, pp. 375–377, Feb. 2015.
- [22] L. Yong, S. Hongbiao, L. Hai, C. Dunjun, Z. Rong, and Z. Youdou, "Field plate engineering for GaN-based Schottky barrier diodes," *J. Semicond.*, vol. 34, no. 5, 2013, Art. no. 054007.
- [23] M.-W. Ha, S.-C. Lee, Y.-H. Choi, S.-S. Kim, C.-M. Yun, and M.-K. Han, "New GaN Schottky barrier diode employing a trench on AlGaN/GaN heterostructure," *Superlattices Microstructures*, vol. 40, nos. 4–6, pp. 567–573, 2006.
- [24] H. Fukushima *et al.*, "Vertical GaN p–n diode with deeply etched mesa and capability of avalanche breakdown," *Appl. Phys. Exp.*, vol. 12, no. 2, 2019, Art. no. 026502.
- [25] S.-C. Lee *et al.*, "High breakdown voltage GaN Schottky barrier diode employing floating metal rings on AlGaN/GaN hetero-junction," in *Proc. IEEE 17th Int. Symp. Power Semicond. Devices ICs (ISPSD)*, 2005, pp. 247–250.
- [26] M. Bhatnagar, H. Nakanishi, S. Bothra, P. McLarty, and B. Baliga, "Edge terminations for SiC high voltage Schottky rectifiers," in *Proc. IEEE 5th Int. Symp. Power Semicond. Devices ICs*, 1993, pp. 89–94.
- [27] S.-C. Chang, S.-J. Wang, K.-M. Uang, and B.-W. Liou, "Design and fabrication of high breakdown voltage 4H-SiC Schottky barrier diodes with floating metal ring edge terminations," *Solid-State Electron.*, vol. 49, no. 3, pp. 437–444, 2005.
- [28] Z. Hu *et al.*, "The investigation of β-Ga<sub>2</sub>O<sub>3</sub> Schottky diode with floating field ring termination and the interface states," *ECS J. Solid-State Sci. Technol.*, vol. 9, no. 2, 2020, Art. no. 025001.
- [29] T.-H. Yang *et al.*, "Temperature-dependent electrical properties of β-Ga<sub>2</sub>O<sub>3</sub> Schottky barrier diodes on highly doped single-crystal substrates," *J. Semicond.*, vol. 40, no. 1, 2019, Art. no. 012801.
- [30] H. Fu, X. Huang, H. Chen, Z. Lu, I. Baranowski, and Y. Zhao, "Ultra-low turn-on voltage and on-resistance vertical GaN-on-GaN Schottky power diodes with high mobility double drift layers," *Appl. Phys. Lett.*, vol. 111, no. 15, 2017, Art. no. 152102.
- [31] F. Iucolano, F. Roccaforte, F. Giannazzo, and V. Raineri, "Barrier inhomogeneity and electrical properties of Pt/GaN Schottky contacts," *J. Appl. Phys.*, vol. 102, no. 11, 2007, Art. no. 113701.
- [32] N. Subramaniyam, M. Sopanen, H. Lipsanen, C.-H. Hong, and E.-K. Suh, "Inhomogeneous barrier height analysis of (Ni/Au)–InAlGaN/GaN Schottky barrier diode," *Jpn. J. Appl. Phys.*, vol. 50, no. 3R, 2011, Art. no. 030201.
- [33] J.-H. Shin, J. Park, S. Jang, T. Jang, and K. Sang Kim, "Metal induced inhomogeneous Schottky barrier height in AlGaN/GaN Schottky diode," *Appl. Phys. Lett.*, vol. 102, no. 24, 2013, Art. no. 243505.
- [34] D. Ewing *et al.*, "Inhomogeneities in Ni/4 H-Si C Schottky barriers: Localized fermi-level pinning by defect states," *J. Appl. Phys.*, vol. 101, no. 11, 2007, Art. no. 114514.
- [35] D. H. Lee, K. Nomura, T. Kamiya, and H. Hosono, "Diffusion-limited a-IGZO/Pt Schottky junction fabricated at 200°C on a flexible substrate," *IEEE Electron Device Lett.*, vol. 32, no. 12, pp. 1695–1697, Dec. 2011.
- [36] J. H. Werner and H. H. Gütter, "Barrier inhomogeneities at Schottky contacts," *J. Appl. Phys.*, vol. 69, no. 3, pp. 1522–1533, 1991.
- [37] Y. Son and R. L. Peterson, "The effects of localized tail states on charge transport mechanisms in amorphous zinc tin oxide Schottky diodes," *Semicond. Sci. Technol.*, vol. 32, no. 12, 2017, Art. no. 12LT02.
- [38] H. von Wenckstern, G. Biehne, R. A. Rahman, H. Hochmuth, M. Lorenz, and M. Grundmann, "Mean barrier height of Pd Schottky contacts on ZnO thin films," *Appl. Phys. Lett.*, vol. 88, no. 9, 2006, Art. no. 092102.
- [39] L. Yu, Q. Liu, Q. Xing, D. Qiao, S. Lau, and J. Redwing, "The role of the tunneling component in the current–voltage characteristics of metal-GaN Schottky diodes," *J. Appl. Phys.*, vol. 84, no. 4, pp. 2099–2104, 1998.